Neurobiology of Disease

Identification of the Upward Movement of Human CSF *In Vivo* and its Relation to the Brain Venous System

Steffi Dreha-Kulaczewski,[1] Arun A. Joseph,[3,4] Klaus-Dietmar Merboldt,[3] Hans-Christoph Ludwig,[2] Jutta Gärtner,[1] and Jens Frahm[3,4]

[1]Department of Pediatrics and Adolescent Medicine, Division of Pediatric Neurology, and [2]Department of Neurosurgery, Division of Pediatric Neurosurgery, University Medical Center Göttingen, 37075 Göttingen, Germany, [3]Biomedizinische NMR Forschungs GmbH am Max-Planck-Institut für biophysikalische Chemie, 37077 Göttingen, Germany, and [4]German Center for Cardiovascular Research, Partner Site Göttingen, Germany

CSF flux is involved in the pathophysiology of neurodegenerative diseases and cognitive impairment after traumatic brain injury, all hallmarked by the accumulation of cellular metabolic waste. Its effective disposal via various CSF routes has been demonstrated in animal models. In contrast, the CSF dynamics in humans are still poorly understood. Using novel real-time MRI, forced inspiration has been identified recently as a main driving force of CSF flow in the human brain. Exploiting technical advances toward real-time phase-contrast MRI, the current work analyzed directions, velocities, and volumes of human CSF flow within the brain aqueduct as part of the internal ventricular system and in the spinal canal during respiratory cycles. A consistent upward CSF movement toward the brain in response to forced inspiration was seen in all subjects at the aqueduct, in 11/12 subjects at thoracic level 2, and in 4/12 subjects at thoracic level 5. Concomitant analyses of CSF dynamics and cerebral venous blood flow, that is, in epidural veins at cervical level 3, uniquely demonstrated CSF and venous flow to be closely communicating cerebral fluid systems in which inspiration-induced downward flow of venous blood due to reduced intrathoracic pressure is counterbalanced by an upward movement of CSF. The results extend our understanding of human CSF flux and open important clinical implications, including concepts for drug delivery and new classifications and therapeutic options for various forms of hydrocephalus and idiopathic intracranial hypertension.

Key words: **CSF; human; *in vivo* flow; phase-contrast real-time MRI; respiration**

Significance Statement

Effective disposal of brain cellular waste products via CSF has been demonstrated repeatedly in animal models. However, CSF dynamics in humans are still poorly understood. A novel quantitative real-time MRI technique yielded *in vivo* CSF flow directions, velocities, and volumes in the human brain and upper spinal canal. CSF moved upward toward the head in response to forced inspiration. Concomitant analysis of brain venous blood flow indicated that CSF and venous flux act as closely communicating systems. The finding of a human CSF–venous network with upward CSF net movement opens new clinical concepts for drug delivery and new classifications and therapeutic options for various forms of hydrocephalus and ideopathic intracranial hypertension.

Introduction

Apart from supporting protection against blows and heat (Zenker et al., 1996), a critical role of CSF is the maintenance of immunologic and biochemical homeostasis and the supply of microenvironments essential for brain health and function. The choroid plexus (CP) adhering to the walls of the brain ventricular system controls the blood–CSF barrier and tightly regulates CSF composition. Multiple bidirectional transport systems within the CP facilitate both secretion of essential ions and molecules into and clearance of unnecessary components out of the CSF into the blood (Spector et al., 2007; Schwartz et al., 2012; Fu et al., 2014). In addition, reports in rodents describe brain-wide perivascular pathways that support the exchange of CSF and interstitial brain fluids primarily for clearance of metabolic waste products. In this model, the pulsation of penetrating cortical arteries drives the CSF along para-arterial routes into brain tissue while it leaves via paravenous spaces after passing the intersti-

Received Aug. 31, 2016; revised Jan. 13, 2017; accepted Jan. 18, 2017.

Author contributions: S.D.-K., H.-C.L., J.G., and J.F. designed research; S.D.-K., A.A.J., K.-D.M., and J.F. performed research; S.D.-K., A.A.J., K.-D.M., and J.F. analyzed data; S.D.-K., A.A.J., J.G., and J.F. wrote the paper.

The work was supported by the Dorothea Schloezer Program of the Georg-August-University Göttingen, Germany (S.D.-K.).

The authors declare no competing financial interests.

Correspondence should be addressed to Steffi Dreha-Kulaczewski, Department of Pediatrics and Adolescent Medicine, Division of Pediatric Neurology, University Medical Center Göttingen, Robert-Koch-Str. 40, 37075 Göttingen, Germany. E-mail: sdreha@gwdg.de.

DOI:10.1523/JNEUROSCI.2754-16.2017

 0270-6474/17/372395-08$15.00/0

tial space (Iliff et al., 2013a, 2013b; Xie et al., 2013). So far, the majority of CSF flow and transport processes have been studied in animal models, whereas clinically relevant CSF dynamics in humans are still poorly understood.

CSF is contained within the human brain ventricular system, which is formed by four interconnected cavities and the subarachnoid spaces between the outer brain surface and skull. The latter communicate freely with the large subarachnoid spaces of the spinal canal via the foramen magnum at the craniocervical junction. Recently, we identified forced inspiration as a major regulator of human CSF flow by applying a novel real-time MRI technique (Dreha-Kulaczewski et al., 2015). In contrast to earlier work using phase-contrast flow MRI techniques with cardiac gating (Greitz et al., 1993; Stadlbauer et al., 2010), the CSF flow related to heartbeat was found to represent only a minor component of the total flow. The unique possibility of measuring CSF dynamics directly by real-time MRI at high spatial and temporal resolution allowed for its evaluation independent of the assumption of any periodicity and thus disclosed inspiration as the dominating driving force (Dreha-Kulaczewski et al., 2015). However, the previously applied real-time MRI method only enabled qualitative identification of flow perpendicular through the imaging section, which precluded more relevant quantitative evaluations of respiratory-driven CSF flux. Our current study uses further methodologic advances toward real-time phase-contrast (i.e., velocity-encoded) flow MRI, which evaluates flow without any implicit dependence on the cardiac cycle; that is, without ECG synchronization. The method provides, for the first time, quantitative access to CSF flow directions, flow velocities, and net flow volumes *in vivo* during respiratory cycles.

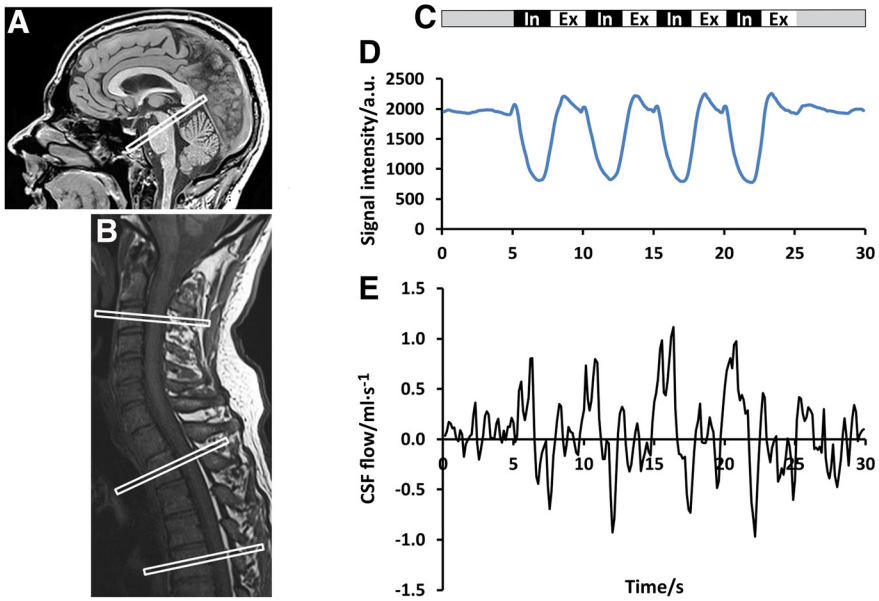

Figure 1. Study design. Left, Midsagittal T1-weighted image of the head (***A***) with ROI for CSF flow in the aqueduct and the cervical and upper thoracic spine (***B***) with ROIs at C3, Th2, and Th5. ***C***, Right, Study protocol comprising 4 cycles of 2.5 s forced inspiration (In) and expiration (Ex) each. ***D***, Corresponding signal intensity of an ROI covering parts of the thoracic wall. ***E***, CSF flow ($ml \cdot s^{-1}$) within the spinal canal at Th5.

Materials and Methods

Subjects. We enrolled 12 healthy volunteers (age range 22–54 years, 7 females, 5 males) without contraindication for MRI and no known illness. The study was approved by the institutional review board and written informed consent was obtained from each subject before MRI. This study was in compliance with the Declaration of Helsinki.

Study design. Four ROIs were selected covering the ventricular CSF system of the brain at the aqueduct and the subdural CSF spaces of the spinal canal at cervical level 3 (C3) and thoracic level 2 (Th2) and Th5 (Fig. 1*A*,*B*). The simultaneous analysis of CSF and venous flow required a venous vessel with a noncollapsible lumen during deep inhalation. Therefore, a respective ROI was placed in one of the prominent veins commonly found at C3 within the internal vertebral venous plexus occupying the spinal epidural space.

During the study, all subjects were asked to follow a predefined breathing protocol (Fig. 1*C*) with 5 s of normal breathing at rest, followed by 4 cycles of 2.5 s of forced inspiration and 2.5 s of forced expiration, respectively, and again 5 s of normal breathing. Two scans for each ROI accounted for intrasubject reproducibility. During MRI in a supine position, all subjects were monitored via ECG. Adherence to the breathing protocol was verified by comparing the movement of the thoracic wall at level Th5 with the timing of the protocol and the simultaneous CSF flow. Corresponding signal intensity changes and CSF flow rates in response to breathing (Fig. 1*D*) demonstrate elevation and lowering of the thoracic wall, as well as positive (i.e., upward) and negative (i.e., downward) CSF flow (Fig. 1*E*) parallel to inspiration and expiration.

Real-time MRI. Real-time phase-contrast flow MRI was performed at 3 Tesla (Magnetom Prisma Fit; Siemens Healthcare). The previously developed method for real-time MRI combines highly undersampled radial FLASH acquisitions with iterative image reconstruction by regularized nonlinear inversion (NLINV) (Uecker et al., 2010). More recently, these real-time capabilities could be extended to flow MRI (Joseph et al., 2012, 2014; Untenberger et al., 2016), which requires the acquisition of two high-speed images with differential velocity encodings perpendicular to the imaging section. For quantitative flow MRI in the brain and spinal canal at high spatial resolution, acquisitions with asymmetric echoes and full motion compensation (Untenberger et al., 2016) were adapted to the following parameters: TR 5.19 ms, TE 4.36 ms, section thickness 5 mm, flip angle 10°, echo asymmetry 30% (50% = symmetry), and 13 radial spokes per image. Therefore, the measurement time for a pair of two flow-encoded images resulted in 135 ms, which defines the temporal resolution of the CSF flow study. An FOV of $192 \times 192\ mm^2$ with a base resolution of 160×160 yielded an in-plane resolution of $1.2 \times 1.2\ mm^2$. The bidirectional velocity sensitivity was adjusted to a velocity-encoding gradient strength (VENC) of 10–20 $cm \cdot s^{-1}$ according to the CSF flow prevalent at different regions. For example, for most subjects, flow at levels Th2 and Th5 was measured with VENC = 20 $cm \cdot s^{-1}$. While acquisitions at the brain aqueduct and spinal C3 region used the 64-channel head coil, CSF flow at Th2 and Th5 were measured by combining an 18-element thorax coil with suitable portions of the 32-element spine coil.

Online reconstruction of phase-contrast velocity maps was performed using a parallelized version of the NLINV algorithm (Schaetz et al., 2012), which was implemented on a bypass computer (sysGen/TYAN Octuple-GPU, 2 × 123 Intel Westmere E5620 processor, 48 GB RAM; Sysgen) to the commercial MRI system. The bypass computer is fully integrated with the host computer and consists of two processors (CPUs, SandyBridge E5-2650; Intel) and eight graphical processing units (GPUs, GeForce GTX TITAN; Nvidia). Immediately after reconstruction, the real-time magnitude images and phase-contrast maps were sent to the host scanner and currently viewed at a rate of 3.5 frames per second (fps); acquisitions were performed at 7.4 fps.

Data analysis. Quantitative analyses of the real-time flow data were performed using CAIPI prototype software (Fraunhofer MEVIS) espe-

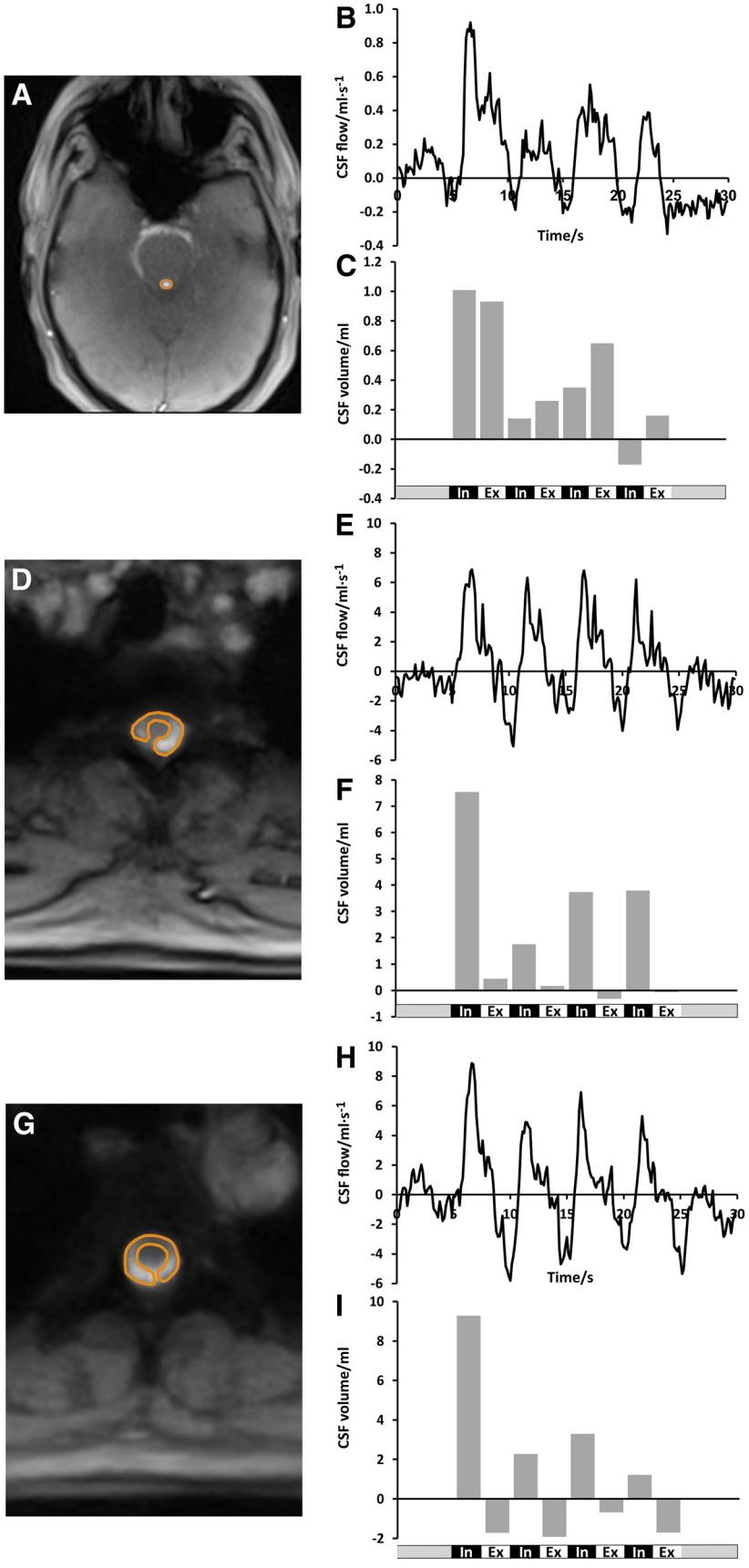

Figure 2. CSF flow in the aqueduct and spinal canal. Magnitude images and ROI definitions (left) and the corresponding CSF flow (ml · s $^{-1}$) and CSF volume (ml) (right) during the breathing protocol in the aqueduct (***A–C***), at Th2 (***D–F***), and at Th5 (***G–I***). In all locations, forced inspiration elicits CSF flow in an upward direction (bright signal). Smaller downward flow occurs at the end of expiration best visible at Th5.

cially developed for the analysis of real-time MRI data; that is, with respect to fully automatic propagation of vessels or myocardial segmentation (Chitiboi et al., 2014). For each analysis, a single ROI was determined manually according to the area of strongest flow signal in magnitude images and phase-contrast maps. Individual anatomic conditions led to considerable variations of ROI sizes and shapes as illustrated in Figures 2*A*, *D*, *G*, and 3*D*, *H*, *L*. Flow values from four cycles of forced inspiration and expiration were summed to yield corresponding volumes per respiratory phase (Tables 1 and 2). Further, temporal filtering of flow data was applied to three selected datasets (for visual inspection only) to remove the effects of cardiac pulsation on CSF flow and thereby demonstrate the relevance of respiratory-related CSF flow even in the presence of strong cardiac-related pulsations. This was accomplished by a low-pass filter with a window of seven images (945 ms) as depicted in Figure 3*B*,*F*,*J* (corresponding unfiltered data are shown in Fig. 3*A*,*E*,*I*). The procedure served to unravel smaller respiration-induced changes in CSF flow for poor breathing performers.

Results

CSF flow

To link the present results to our preceding qualitative study of CSF dynamics, we first performed quantitative flow MRI at the level of the aqueduct (Fig. 2*A*). In contrast to other parts of the brain ventricular system, this small channel between the third and fourth ventricle best meets the requirements for a reliable velocity-encoded phase-contrast MRI study of through-plane flow, namely the predominance of unidirectional laminar flow with constant velocity. In fact, the absence of any useful phase-contrast flow MRI signal in the lateral and third ventricle must be attributed to the occurrence of more complex flow in these large cavities (Yamada et al., 2008). All measurements in the spinal canal revealed comparable results to those in the aqueduct due to physical conditions consistent with the assumptions underlying phase-contrast flow MRI.

Figures 2*A*,*D*,*G*, show representative anatomic structures and definitions of the ROIs in the aqueduct, Th2, and Th5. Intersubject differences reflect the variability in local anatomic and hemodynamic conditions. In full agreement with our preceding study, the results again confirm that CSF flow is strongly affected by forced respiration, whereas cardiac-related flow represents a consistent though minor low-amplitude contribution. Most importantly, "positive" CSF velocities at the onset of every forced inspiration refer to a pronounced upward flow into the head (bright signal). This di-

Table 1. CSF volume (ml) during forced breathing: aqueduct and upper thoracic spinal canal

		Aqueduct			Th2			Th5		
Subject	Scan	Inspiration	Expiration	Net volume	Inspiration	Expiration	Net volume	Inspiration	Expiration	Net volume
#1	1	1.3	2.0	3.3	16.5	−1.4	15.1	20.5	−9.9	10.6
	2	1.8	1.5	3.3	16.8	0.1	16.9	16.1	−6.0	10.1
#2	1	0.2	0.3	0.5	0.7	0.4	1.1	0.2	−1.4	−1.2
	2	0.4	0.6	1.0	0.3	1.2	1.5	−0.4	−0.3	−0.7
#3	1	0.5	0.4	0.9	1.1	0.9	2.0	0.4	−0.8	−0.4
	2	0.7	0.3	1.0	1.8	0.6	2.4	1.9	−0.7	1.2
#4	1	0.2	0.1	0.3	1.8	−0.6	1.2	2.4	−3.5	−1.1
	2	0.2	0.1	0.3	2.0	−0.3	1.7	1.4	−2.7	−1.3
#5	1	1.3	1.0	2.3	−1.4	−1.0	−2.4	−0.4	−0.2	−0.6
	2	1.1	1.2	2.3	−3.1	−3.4	−6.5	−0.5	0.1	−0.4
#6	1	0.4	0.2	0.6	2.7	−0.4	2.3	2.6	−1.3	1.3
	2	0.3	0.2	0.5	1.4	0.1	1.5	2.9	−1.2	1.7
#7	1	0.4	0.3	0.7	0.2	1.3	1.5	0.0	0.0	0.0
	2	0.7	0.4	1.1	0.5	−0.2	0.3	0.3	−1.8	−1.5
#8	1	0.1	0.0	0.1	1.0	0.3	1.3	0.1	−1.5	−1.4
	2	0.2	0.0	0.2	0.7	1.4	2.1	1.6	−0.8	0.8
#9	1	1.0	−0.4	0.6	5.7	−1.3	4.4	2.0	−0.6	1.4
	2	1.9	−0.2	1.7	5.7	−1.1	4.6	1.7	−0.3	1.4
#10	1	0.4	0.1	0.5	4.7	0.5	5.2	1.9	−1.4	0.5
	2	0.4	0.1	0.5	2.8	−1.2	1.6	Not performed		
#11	1	0.5	0.1	0.6	3.6	1.0	4.6	1.5	−2.0	−0.5
	2	0.4	0.1	0.5	3.2	0.6	3.8	2.3	−3.5	−1.2
#12	1	0.4	−0.2	0.2	1.6	−1.2	0.4	0.0	0.0	0.0
	2	0.5	−0.3	0.2	1.8	−1.1	0.7	1.1	−1.6	−0.5
Mean ± SD[a]		0.6 ± 0.5	0.3 ± 0.6	1.0 ± 0.9	3.0 ± 4.6	−0.2 ± 1.1	2.8 ± 4.7	2.6 ± 5.1	−1.8 ± 2.3	1.0 ± 3.2

[a]Averaged across subjects.

Table 2. CSF and venous blood volume (ml) during forced breathing at C3

		C3 subdural CSF		C3 epidural vein	
Subject	Scan	Inspiration	Expiration	Inspiration	Expiration
#1	1	16.7	−4.8	−4.4	−1.9
	2	12.0	−0.1	−2.6	−1.4
#2	1	0.8	1.0	−7.4	−3.0
	2	0.4	2.3	−4.3	−1.2
#3	1	NA		NA	
	2	2.6	1.5	−2.0	−1.7
#4	1	0.9	0.1	−0.2	−0.1
	2	1.0	−0.4	−0.2	−0.1
#5	1	1.5	1.6	−3.3	−3.9
	2	0.7	2.0	NA	
#6	1	2.5	0.0	−1.5	−1.4
	2	2.9	1.0	NA	
#7	1	2.9	0.7	−0.7	−0.2
	2	2.0	1.3	−1.0	−0.4
#8	1	1.2	0.6	−1.8	−1.4
	2	2.2	0.4	−1.7	−1.4
#9	1	1.3	0.7	−0.2	−0.7
	2	3.4	−0.6	−0.2	−0.4
#10	1	4.9	0.7	NA	
	2	7.4	−0.5	−0.5	−0.5
#11	1	1.9	0.6	−2.1	−1.8
	2	1.6	0.2	−1.9	−1.8
#12	1	2.6	−0.1	−0.4	−0.4
	2	3.1	−0.9	−0.3	−0.3
Mean ± SD		3.3 ± 3.9	0.3 ± 1.4	−1.8 ± 1.9	−1.2 ± 1.0

NA, Not analyzed due to low SNR.

rection could be reproduced both in the intracranial CSF system and spinal canal (Fig. 2*B*,*E*,*H*). Conversely, forced expiration resulted in "negative" velocities that reflect a reversal of direction with CSF flow pointing downward, albeit to a markedly variable extent (dark signal). Total CSF volumes for forced inspiration and expiration clearly depict the dominant upward directionality (Fig. 2*C*,*F*,*I*) with some reverse (i.e., downward) flow during expiration at level Th5 (Fig. 2*I*).

Within our group of subjects, we observed considerable intersubject differences in performance. For example, Figure 3 depicts the CSF flow pattern at level Th2 for three subjects who present with a clear increase during forced inspiration (Fig. 3*A*), pronounced fluctuation (Fig. 3*E*), and strong cardiac-related pulsation (Fig. 3*I*). Cardiac-related CSF flow reflects variations in the local anatomic and hemodynamic situation, which not only determines the size and shape of the individual ROI, but also alters the sensitivity to arterial pulsations. Nevertheless, the application of a low-pass filter (Fig. 3*B*,*F*,*J*) confirms the underlying respiration-related flow pattern in all three cases, with consistent CSF flow upward during forced inspiration. This same pattern was obtained for the corresponding total CSF flow volumes (Fig. 3*C*,*G*,*K*) integrated over the individual respiratory cycles of the unfiltered data.

The total CSF flow volumes of all subjects are summarized in Table 1 for the aqueduct, Th2, and Th5. Subject #1, a long-standing saxophone player, achieved exceptional high values, presumably because of his intense and reproducible breathing performance. In 12/12 subjects, the CSF net flow through the aqueduct, that is, the sum of total inspiratory and expiratory flow volumes, was positive. This observation again implies that, during 20 s of deep breathing, CSF moves upward from the fourth into the third ventricle. In the spinal canal, a net CSF flow in upward direction was seen in 11/12 subjects at Th2 and 3/12 subjects at Th5 in both scans. Negative CSF net flow volumes were detected at Th2 in one subject (#5) and at Th5 in four subjects (#2, #4, #5, #11). At Th5, two subjects (#3, #8) revealed opposite CSF net flow in both scans and subjects #7 and #12 revealed negative CSF net flow in one of the scans and none in the other. In one subject only, due to time constraints, a single scan was obtained at Th5 and demonstrated positive net flow.

The mean CSF flow volume of all subjects during deep inspiration was positive in all three ROIs (Table 1, bottom row), substantiating the observation of an upward direction in the in-

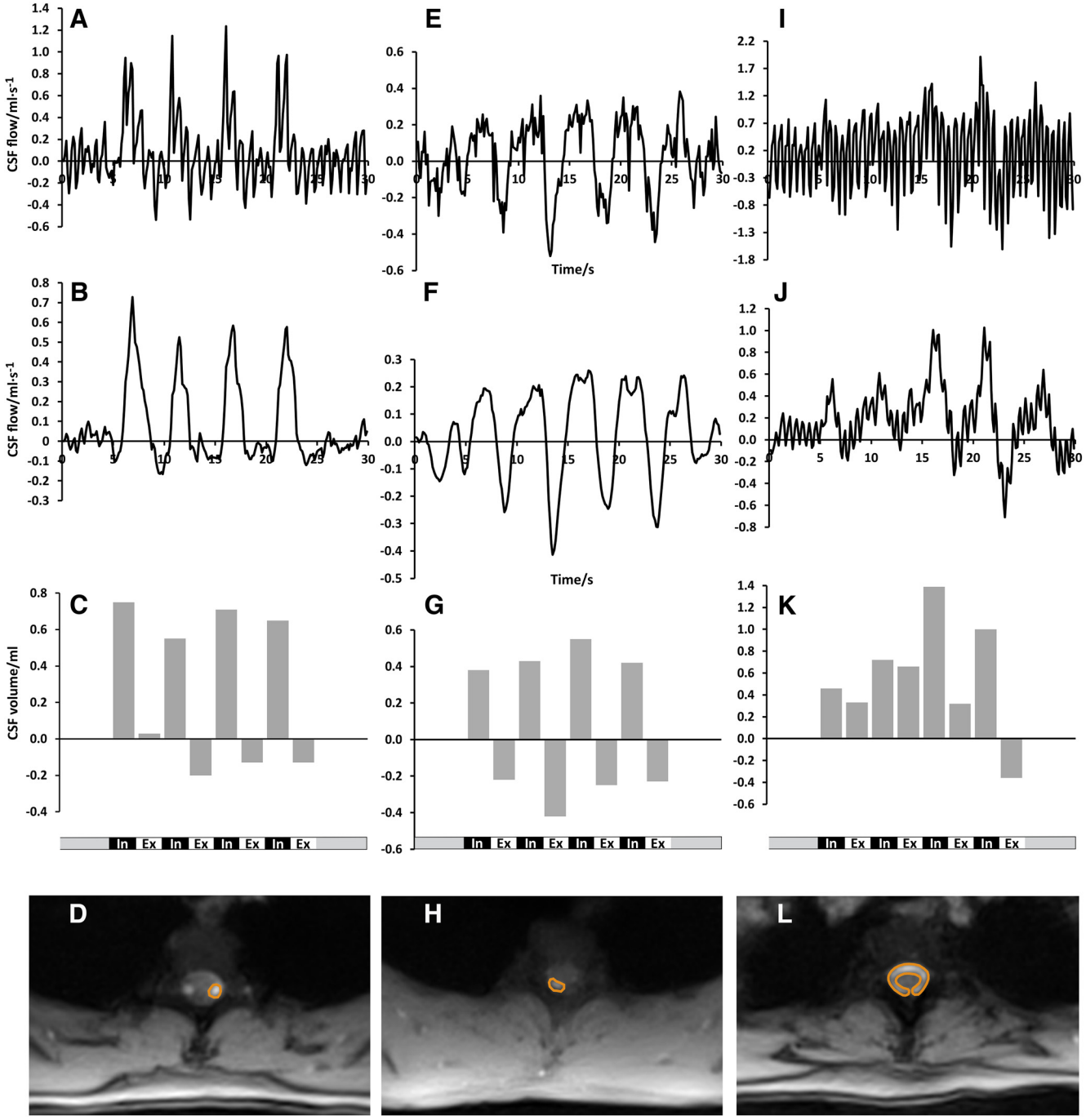

Figure 3. CSF flow at Th2 for three different subjects. Top, CSF flow (ml · s $^{-1}$); second row, CSF flow (ml · s $^{-1}$) with a low-pass filter; third row, CSF flow volume (ml) at Th2 during the breathing protocol for subject #6 (***A–C***), subject #12 (***E–G***), and subject #11 (***I–K***). Bottom, Magnitude images and ROI definitions for subject #6 (***D***), subject #12 (***H***), and subject #11 (***L***). Despite different performance quality and ROI sizes, all subjects reveal CSF flow in an upward direction in response to inspiration.

dividual subject. Moreover, the mean of CSF net flow volumes during 20 s of forced respiration yielded positive values, confirming the finding that CSF preferably moves toward the head and up the ventricular system during inspiration.

Venous blood flow

The observation of CSF net flow into rather than out of the head appears counterintuitive in view of its main production side at the CP within the brain ventricles and its role of draining the brain from waste products. Therefore, to further explore this finding, we turned our attention to the vascular systems of brain and neck. In particular, the venous backflow from the cranial and cervical regions to the heart is governed by respiration-induced changes of intrathoracic pressure. The knowledge that lowering of the intrathoracic pressure during inspiration affects flow dynamics in cervical veins directly led us to look into venous flow dynamics. Using real-time phase-contrast flow MRI, we could observe that the large veins of the neck (e.g., internal and external jugular veins) collapsed as a result of the sudden intrathoracic pressure reduction with onset of every forced inspiration, which renders them inapt for flow evaluations. However, the prominent vessels of the internal vertebral venous plexus in the epidural

spaces of the upper cervical spinal canal, the posterior venous drainage pathway of the brain, were suitable for an ROI-based flow analysis. Figure 4*A* illustrates the ROI placements in the subdural CSF space and in a well definable, eminent vein within the spinal epidural space at C3 (Fig. 4*A*,*B*). Flow MRI analysis revealed continuous negative (i.e., downward) flow out of the head as expected. With the onset of every forced inspiration, an increase of the venous outflow was observed, which resulted in an augmented venous blood volume leaving the head (Fig. 4*C*,*D*).

CSF and venous blood fluid system

The phase-contrast velocity map at C3 (Fig. 4*B*) unequivocally demonstrates the concurrent opposite flow directions of subdural CSF (upward/bright signal) and epidural venous blood (downward/dark signal) during deep inhalation. Every forced inspiration induces pronounced CSF flow up into the head (Fig. 4*E*,*F*) and simultaneously enhances venous outflow. Figure 5 illustrates the almost instantaneous response of both fluid systems to the respiration-related pressure changes in the upper chest as the underlying common source.

Table 2 displays the total CSF and venous blood flow volumes of all 12 subjects at C3. Note that all studies revealed positive CSF flow volume (mean 3.3 ± 3.9 ml) during forced inspiration, while expiratory CSF flow volumes were much smaller or even slightly negative (mean 0.3 ± 1.4 ml). Negative venous blood flow volume was greater during deep inspiration (mean −1.8 ± 1.9 ml) than during expiration (mean −1.2 ± 1.0 ml) in 17/20 studies. Interestingly, subject #5 (scan 1), who presented with a more negative venous blood flow volume during deep expiration, also showed a larger upward CSF flow volume simultaneously (Table 2).

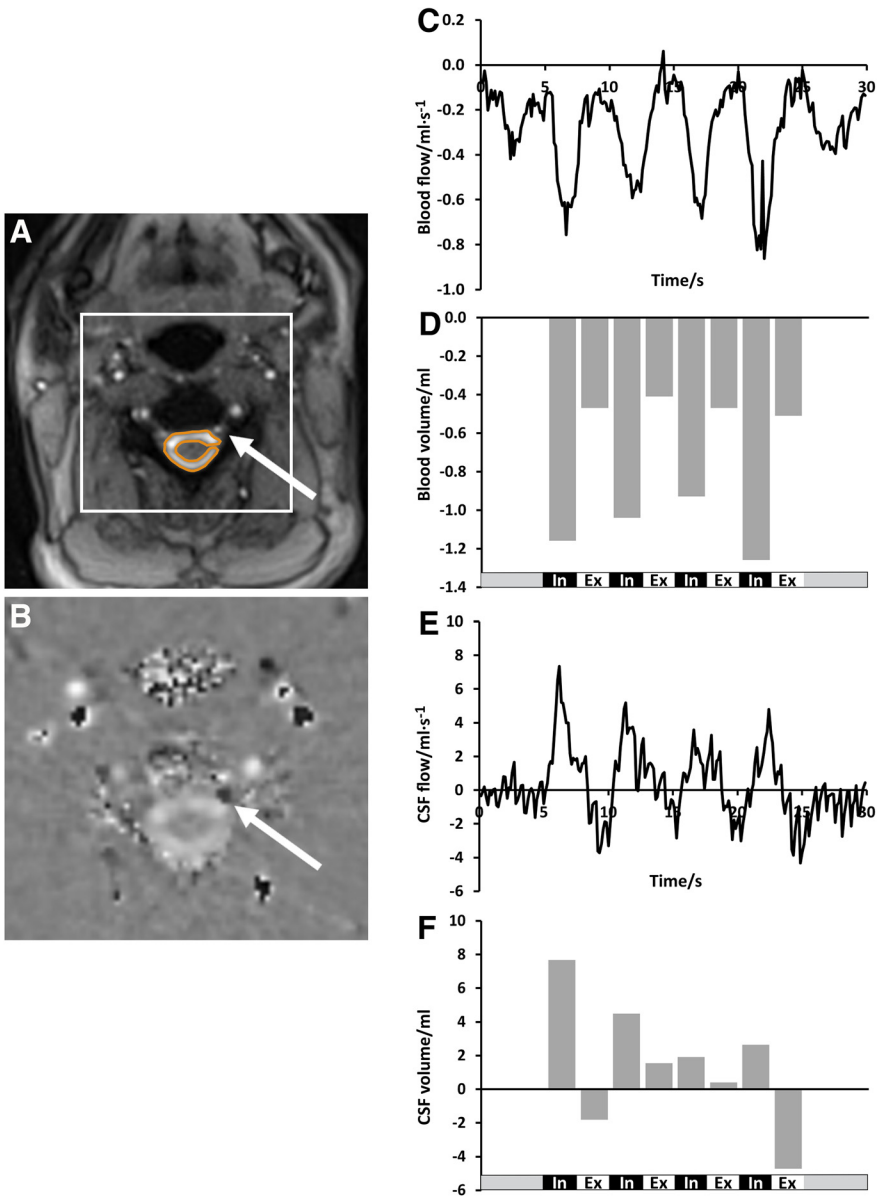

Figure 4. Venous blood flow and simultaneous CSF flow at C3. Left, Magnitude image with ROI in subdural CFS space; arrow pointing towards left epidural vein (***A***) and magnified phase-contrast velocity map with ROI in left epidural vein (***B***, arrow). Dark signal in the vein (arrow) encodes downward flow and the bright signal in the CSF space indicates upward flow. Right, "Negative" (i.e., downward) blood flow (ml · s $^{-1}$) (***C***) and blood volume (ml) (***D***) in epidural veins out of the head as well as concomitant "positive" (i.e., upward) CSF flow (ml · s $^{-1}$) (***E***) and CSF volume (ml) (***F***) during the breathing protocol (bottom traces). Note that many blood vessels of the neck display phase wraps (black signal spots) because flow is too fast here for the sequence parameter adjusted to slower CSF dynamics.

Discussion

The advancement of high-resolution real-time MRI to quantitative flow studies enabled us to measure CSF and venous blood flow concurrently for the first time at adequate spatiotemporal resolution and without the need for cardiac synchronization.

In agreement with our initial study, forced inspiration elicited a prompt and significant increase of CSF flow. To our initial surprise, however, this inspiratory increase of CSF flux was directed upward, not only in the upper cervical and upper and middle thoracic spine, but also in the aqueduct as part of the ventricular system of the brain. These results were consistent regardless of size or shape of the chosen ROI and were even true in the few studies with an apparent dominance of cardiac-related CSF flow. The resulting inspiration-induced CSF flow volumes yielded positive values for the vast majority of measurements verifying the upward movement at all locations. Forced expiration rendered CSF flow considerably more variable at the different positions studied. At the lowest level, Th5 negative expiratory CSF flow volumes prevailed, indicating a downward movement in individual subjects. Nevertheless, the net flow volumes of all subjects were positive in all ROIs, supporting the notion of a net upward movement of CSF.

Pulsatile movements of CSF dependent on heartbeat and respiration in humans have been observed previously (Du Boulay, 1966; Williams, 1981; Greitz et al., 1993). For example, during early myelography, respiratory movements of the jodipine column inside the dura led to a raise under inspiration and a descent under expiration (Reitan, 1941). Since the advent of flow-

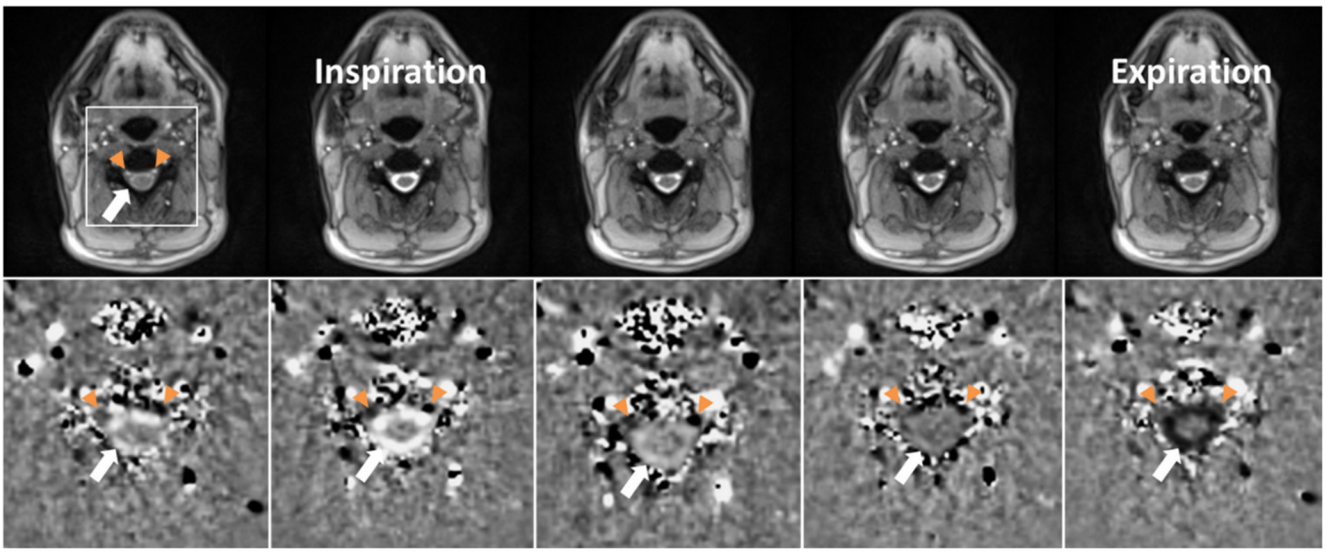

Figure 5. CSF flow and simultaneous venous blood flow at C3 during one respiratory cycle (inspiration and expiration). Serial magnitude images (top) and corresponding phase-contrast velocity maps from left to right (bottom) were selected from a real-time MRI video at 135 ms temporal resolution (every seventh frame, period of 3.78 s, subject #1). Bright CSF flow velocities in the ring-like subdural spinal space (white arrow) indicate upward movement with onset of forced inspiration. Concurrently, the epidural veins (left more than right) (orange arrowheads) exhibit a remarkably dark (i.e., downward) flow signal. During expiration, the CSF flow direction is reversed (dark signal) and the velocity of the epidural veins diminishes (dark signal less pronounced).

sensitive MRI sequences, only very few studies avoided cardiac synchronization to evaluate the effects of respiration on CSF dynamics using echoplanar imaging (Klose et al., 2000; Friese et al., 2004) or respiration-induced spin labeling (Yamada et al., 2013). A more recent study used real-time phase-contrast flow MRI based on echoplanar imaging to evaluate the effect of different breathing maneuvers (Chen et al., 2015). The investigators reported a strong and variable cardiac-related component and, in agreement with our present findings, suggest that breathing leads to an upward-directed CSF velocity in the inspiration phase.

Apart from respiration and cardiac pulsation, muscular movements have been suggested as being another contributor to CSF circulation after comparing ECG-synchronized flow MRI data before and after a 1 min head rotation period (Xu et al., 2016). However, because such exercises are also accompanied by enforced breathing, it will be difficult to assess any direct effect of muscular pumping. Moreover, one may speculate that respective influences on CSF flow are likely to be less prominent than exerted by forced inspiration.

The observation of a respiration-driven CSF net movement upward to the head prompted a real-time MRI analysis of the concomitant cerebral venous flow. Venous drainage from the head and cervical regions to the heart is tightly governed by respiration-induced changes of intrathoracic pressure. Consistent with this, we detected an increase of the venous flow out of the head in epidural veins at C3 with the reduction of the intrathoracic pressure during deep inspiration in 10/12 subjects. Venous blood flow volumes reached greater negative values during forced inspiration than during exhalation in all subjects. These findings hold true despite considerable intersubject variability, which was also reported for flow in the sagittal sinus (Gideon et al., 1994) and were ascribed to differences in hydration status, time of day, force exerted for thorax movements, and physical fitness.

Assuming a constant intracranial volume as stated by the Monro–Kellie doctrine (Greitz et al., 1992), the upward CSF flow and the enhanced venous outflow most presumably occur compensatory to each other. This concept is physically plausible, as was suggested previously (Klose et al., 2000; Friese et al., 2004). In view of the instantaneous albeit opposite responses to inspiration, the present results support the notion of a closely communicating and interdependent CSF–venous system.

So far, cardiac-gated MRI studies on the relationship between CSF movement and blood flow have considered, not just periodic events within a heartbeat, but also the large veins of the neck (Greitz et al., 1992; Balédent et al., 2004). However, in all subjects studied here, these vessels temporarily collapsed at the onset of forced inhalation due to the associated lowering of the pressure inside the thoracic cavity. In contrast, spinal epidural veins and venous plexus were much less or not at all affected. These valveless vessels are important constituents of the posterior venous drainage system of the head and possess numerous connections to the veins of the brain inside the skull. They are encased in the bony cavity of the vertebral column and thus are not affected directly by sudden intrathoracic pressure changes. In addition, bridging trabeculae within their lumen further prevent collapse or overdistension of the vessels similar to the large venous sinuses in the skull (Stringer et al., 2012). To our knowledge, this study comprises the first quantitative evaluation of human spinal epidural blood flow *in vivo*.

In conclusion, the fundamental improvement to velocity-encoded real-time MRI now uniquely enables rapid and robust assessment of CSF volumes and flux in the human brain *in vivo*. Our study revealed an upward-directed net CSF movement into the head and further into the brain ventricular system in response to forced inspiration and a tight connection to the venous flow within the head and spinal canal. These findings broaden our understanding of human CSF flux and the communication across cerebral fluid systems significantly. Real-time phase-contrast MRI studies can now be translated into clinical practice to unravel the underlying pathophysiology of CSF and venous flow dynamics in patients with hydrocephalus and associated neurological disorders. Furthermore, future studies will cover the

entire spinal canal to assess the contributions of respiration and cardiac pulsation at different spinal levels.

References

Balédent O, Gondry-Jouet C, Meyer ME, De Marco G, Le Gars D, Henry-Feugeas MC, Idy-Peretti I (2004) Relationship between cerebrospinal fluid and blood dynamics in healthy volunteers and patients with communicating hydrocephalus. Invest Radiol 39:45–55. CrossRef Medline

Chen L, Beckett A, Verma A, Feinberg DA (2015) Dynamics of respiratory and cardiac CSF motion revealed with real-time simultaneous multi-slice EPI velocity phase contrast imaging. Neuroimage 122:281–287. CrossRef Medline

Chitiboi T, Hennemuth A, Tautz L, Huellebrand M, Frahm J, Linsen L, Hahn H (2014) Context-based segmentation and analysis of multi-cycle real-time cardiac MRI. IEEE Int Symp Biomed Imaging 2014:943–946.

Dreha-Kulaczewski S, Joseph AA, Merboldt KD, Ludwig HC, Gärtner J, Frahm J (2015) Inspiration is the major regulator of human CSF flow. J Neurosci 35:2485–2491. CrossRef Medline

Du Boulay GH (1966) Pulsatile movements in the CSF pathways. Br J Radiol 39:255–262. CrossRef Medline

Friese S, Hamhaber U, Erb M, Kueker W, Klose U (2004) The influence of pulse and respiration on spinal cerebrospinal fluid pulsation. Invest Radiol 39:120–130. CrossRef Medline

Fu X, Zhang Y, Jiang W, Monnot AD, Bates CA, Zheng W (2014) Regulation of copper transport crossing brain barrier systems by Cu-ATPases: effect of manganese exposure. Toxicol Sci 139:432–451. CrossRef Medline

Gideon P, Sørensen PS, Thomsen C, Ståhlberg F, Gjerris F, Henriksen O (1994) Assessment of CSF dynamics and venous flow in the superior sagittal sinus by MRI in idiopathic intracranial hypertension: a preliminary study. Neuroradiology 36:350–354. CrossRef Medline

Greitz D, Wirestam R, Franck A, Nordell B, Thomsen C, Ståhlberg F (1992) Pulsatile brain movement and associated hydrodynamics studied by magnetic resonance phase imaging: the Monro-Kellie doctrine revisited. Neuroradiology 34:370–380. CrossRef Medline

Greitz D, Franck A, Nordell B (1993) On the pulsatile nature of intracranial and spinal CSF-circulation demonstrated by MR imaging. Acta Radiol 34:321–328. Medline

Iliff JJ, Lee H, Yu M, Feng T, Logan J, Nedergaard M, Benveniste H (2013a) Brain-wide pathway for waste clearance captured by contrast-enhanced MRI. J Clin Invest 123:1299–1309. CrossRef Medline

Iliff JJ, Wang M, Zeppenfeld DM, Venkataraman A, Plog BA, Liao Y, Deane R, Nedergaard M (2013b) Cerebral arterial pulsation drives paravascular CSF-interstitial fluid exchange in the murine brain. J Neurosci 33:18190–18199. CrossRef Medline

Joseph AA, Merboldt KD, Voit D, Zhang S, Uecker M, Lotz J, Frahm J (2012) Real-time phase-contrast MRI of cardiovascular blood flow using undersampled radial fast low-angle shot and nonlinear inverse reconstruction. NMR Biomed 25:917–924. CrossRef Medline

Joseph A, Kowallick JT, Merboldt KD, Voit D, Schaetz S, Zhang S, Sohns JM, Lotz J, Frahm J (2014) Real-time flow MRI of the aorta at a resolution of 40 ms. J Magn Reson Imaging 40:206–213. CrossRef Medline

Klose U, Strik C, Kiefer C, Grodd W (2000) Detection of a relation between respiration and CSF pulsation with an echoplanar technique. J Magn Reson Imaging 11:438–444. CrossRef Medline

Reitan H (1941) On movements of fluid inside the cerebro-spinal space. Acta Radiologica 22:763–769.

Schaetz S, Uecker M (2012) A multi-GPU programming library for real-time applications: algorithms and architectures for parallel processing. In: Lecture Notes in Computer Science 7439 (Xiang Y, Stojmenovic I, Apduhan BO, Nakano K, Zomaya A, eds), pp 114–128. Berlin Heidelberg: Springer.

Schwartz M, Baruch K (2012) Vaccine for the mind: Immunity against self at the choroid plexus for erasing biochemical consequences of stressful episodes. Hum Vaccin Immunother 8:1465–1468. CrossRef Medline

Spector R, Johanson CE (2007) Vitamin transport and homeostasis in mammalian brain: focus on vitamins B and E. J Neurochem 103:425–438. CrossRef Medline

Stadlbauer A, Salomonowitz E, van der Riet W, Buchfelder M, Ganslandt O (2010) Insight into the patterns of cerebrospinal fluid flow in the human ventricular system using MR velocity mapping. Neuroimage 51:42–52. CrossRef Medline

Stringer MD, Restieaux M, Fisher AL, Crosado B (2012) The vertebral venous plexuses: the internal veins are muscular and external veins have valves. Clin Anat 25:609–618. CrossRef Medline

Uecker M, Zhang S, Voit D, Karaus A, Merboldt KD, Frahm J (2010) Real-time MRI at a resolution of 20 ms. NMR Biomed 23:986–994. CrossRef Medline

Untenberger M, Tan Z, Voit D, Joseph AA, Roeloffs V, Merboldt KD, Schätz S, Frahm J (2016) Advances in real-time phase-contrast flow MRI using asymmetric radial gradient echoes. Magn Reson Med 75:1901–1908. CrossRef Medline

Williams B (1981) Simultaneous cerebral and spinal fluid pressure recordings. I. Technique, physiology, and normal results. Acta Neurochir 58:167–185. CrossRef Medline

Xie L, Kang H, Xu Q, Chen MJ, Liao Y, Thiyagarajan M, O'Donnell J, Christensen DJ, Nicholson C, Iliff JJ, Takano T, Deane R, Nedergaard M (2013) Sleep drives metabolite clearance from the adult brain. Science 342:373–377. CrossRef Medline

Xu Q, Yu SB, Zheng N, Yuan XY, Chi YY, Liu C, Wang XM, Lin XT, Sui HJ (2016) Head movement, an important contributor to human cerebrospinal fluid circulation. Sci Rep 6:31787. CrossRef Medline

Yamada S, Miyazaki M, Kanazawa H, Higashi M, Morohoshi Y, Bluml S, McComb JG (2008) Visualization of cerebrospinal fluid movement with spin labeling at MR imaging: preliminary results in normal and pathophysiologic conditions. Radiology 249:644–652. CrossRef Medline

Yamada S, Miyazaki M, Yamashita Y, Ouyang C, Yui M, Nakahashi M, Shimizu S, Aoki I, Morohoshi Y, McComb JG (2013) Influence of respiration on cerebrospinal fluid movement using magnetic resonance spin labeling. Fluids Barriers CNS 10:36–42. CrossRef Medline

Zenker W, Kubik S (1996) Brain cooling in humans: anatomical considerations. Anat Embryol 193:1–13. Medline